/

Article / Book Information

Title	Rate equation-based numerical analysis of mutual injection for phase locked 2D-VCSEL array using Talbot effect
Author	Taichi Shichijo, Tomoyuki Miyamoto
Citation	Japanese Journal of Applied Physics, vol. 58, no. SJ,
Pub. date	2019, 6
Note	This is the Accepted Manuscript version of an article accepted for publication in Japanese Journal of Applied Physics. IOP Publishing Ltd is not responsible for any errors or omissions in this version of the manuscript or any version derived from it. The Version of Record is available online at https://doi.org/10.7567/1347-4065/ab1b66.

Rate equation-based numerical analysis of mutual injection for phase locked 2D-VCSEL array using Talbot effect

Taichi Shichijo and Tomoyuki Miyamoto*

FIRST, IIR, Tokyo Institute of Technology, Yokohama 226-8503, Japan

E-mail: tmiyamot@pi.titech.ac.jp

Abstract: The operating conditions and structural design that are necessary to realize 2-dimensional (2D) phased-locked VCSEL array using Talbot effect (Talbot-VCSEL) were studied by numerical analysis of mutual injection locking by using the laser rate equation. Analysis of a few elements confirms the tendency of mutual injection locking and shows that the locking range can be expanded by increasing the number of elements which have close wavelength. Furthermore, Talbot-VCSEL of a 2D array was analyzed to clarify the optimal array configuration that are necessary for locking operation. As the results, the aperture diameter of >5 μm and the array size of > 9×9 with 30 μm of array pitch is appropriate minimum configuration of the 2D VCSEL array.

1. Introduction

In recent years a vertical cavity surface emitting laser (VCSEL) array has attracted attention as a high power light source. The VCSEL shows excellent characteristics, such as low threshold and circular beam as a single device, and ease of two-dimensional integration. Although output power of a single device of the typical VCSEL is limited in small of 10 mW order or less, it is possible to obtain a high output power by two-dimensional array integration. Ideally, total output power can be increased proportional to the number of devices in the array. However, since individual VCSEL lases independently in such VCSEL array, beam quality becomes low. If the wavelength and phase of each laser can be locked together, it can be used a laser whose beam shape can easily be controlled. The laser will have good characteristics such as high focusing performance, less diffraction without lens and controllability of beam direction. These lasers are useful for high power applications like optical wireless power transmission,[1-3] laser display, laser lighting, and laser processing including heat treatment, and so on.

In order to lock the wavelength and phase of each laser, which lase independently, there is a method called phase locking. Phase-locked lasers are usually achieved by injection locking in two pairs of lasers as master and slave laser. On the other hand, there is another technology of using tight coupling with next device. For expanding this type of laser to a two-dimensional array or a surface planar operation, a tightly coupled coherent VCSEL array[4-9] using closely spaced elements and a photonic crystal laser[10-13] are reported, respectively. A tightly coupled coherent VCSEL array is phase-locked due to coupling by light leakage between individual VCSELs. Recently, operation of closely spaced lasers are reported. It is necessary to expand the number of devices and the total area for increasing the output power as the next step. A photonic crystal laser, which has the entire structure of the periodic pattern of wavelength scale, operates as one resonator. A single mode beam with a single wavelength, a light output of more than several Watt and a chip size of several hundreds of micrometer square has already been reported.

Since these tightly coupled coherent VCSEL arrays and photonic crystal lasers use strong coupling of light separated by wavelength scale as the principle, it is necessary to fabricate the pitch between the elements and the size of devices very precisely. As the result, since it is difficult to widen the pitch between the elements and heat dissipation of individual lasers

is strongly restricted, reduction of the output density and restriction of characteristics due to heat generation are problems. In addition, when widening the laser chip, nonuniformity of current injection into individual lasers may become a problem due to limitation of the electrode pattern and its width.

Aside from these lasers, VCSEL array, which is coupled by using the Talbot effect (Talbot-VCSEL), was proposed.[14] This Talbot-VCSEL as shown in Fig. 1, is coupled by re-injection the light propagated once outside the device and diffracted. Therefore, some design tolerances of element spacing, and device size can be expected. As the results, it is possible to get excellent characteristics of a whole array, such as variable pitch between VCSELs, promotion of heat dissipation due to pitch expansion and uniform operation due to flexibility of metal electrode pattern. Although such Talbot-VCSEL has already been proposed as described in the next section, it has not been thoroughly considered. In particular, since detailed analyses and designs regarding phase locking conditions have not been performed, appropriate structures and operating conditions are still unknown. For achievement of high performance operation of the Talbot-VCSEL, detailed investigation of operation conditions and appropriate structures is strongly needed.

Based on the above background, this research aims to realize a phase locked VCSEL array using the Talbot effect as an array light source with excellent beam characteristics. In this report, we investigated the operation condition and an effective structural design of Talbot-VCSEL theoretically using numerical simulation. Although a part of this research has been reported in Ref. 15 in MOC2018, we will report detailed analysis methods and analysis conditions including unreported results.

2. Injection Locking in Talbot-VCSEL

Phase locking is achieved by using injection locking. This phenomenon is known as a method, which is injection of a laser light oscillating at a certain wavelength (master laser) into another laser oscillating at a different wavelength (slave laser). The oscillation frequency and phase of the slave laser become the same as that of the master laser in the case that the frequency difference of the two lasers is within a small range corresponding to the intensity of the master laser.[16-19]

This mechanism of the injection locking is as follows. When the light is injected from the

master laser into the slave laser, the electric field of the light in the slave laser increases. Since this situation is similar to the inside of the slave laser with the reflectivity of the laser reflector increased, it is considered to be equivalent to the situation in which the threshold condition of the slave laser is lowered effectively. As a result, the threshold carrier density of the slave laser decreases. When the carrier density decreases, the refractive index increases due to reduction of the carrier plasma effect. Since the optical path length of the cavity becomes longer, the lasing wavelength shifts to the longer wavelength. As the result, the wavelength and phase of the slave laser also converge to that of the master laser and the phase locking state occurs. In typical applications, an isolator is inserted so that the light of the slave laser does not return to the master laser. Without the isolator, these two lasers are under the condition that they mutually affect each other, called mutual injection locking.[20-22]

On the other hand, Talbot effect is a phenomenon in which the light of one-dimensional or orthogonal two-dimensional array constituted by the periodical pattern propagates and interferes. The interference image with exactly same periodical pattern and intensity as the original is re-imaged at the distance as shown below called Talbot distance.[23-26]

$$z_t = {2mp^2}/{\lambda^2} \qquad (1)$$

Here, z_t is the Talbot distance, p is the pitch of the array, and m is an integer. This principle is derived easily by calculation of the Fresnel-Kirchhoff integration with infinite periodic structure. Any complicated pattern can be re-imaged. However, it is necessary that they are constituted by patterns of infinite number of arrays, and their wavelengths and phases are required to be uniform.

Talbot-VCSEL is realized due to mutual injection locking by using Talbot effect for the laser array consists of N×N VCSELs. As shown in Fig. 1, re-imaged light by the Talbot effect is used as the injection light of the mutual injection locking of the VCSEL array by placing a reflector (Talbot-mirror) at half of the Talbot distance. It is assumed that the Talbot-mirror is a flat reflector with a reflectivity of 100%. Although the reflector size is assumed to be infinite in the calculation, the same size as the light source array size is sufficient for the influence on locking. The issue of this configuration is that the complete Talbot re-imaging

is formed only with a coherent light which has infinite number of arrays, uniform wavelength and phase. After phase locking, the latter condition is satisfied, however this phase locking is objective of this configuration. In an actual Talbot-VCSEL device, there are finite number of array size and wavelength detuning between individual elements. Since an analysis of the operating condition such a non-ideal situation of Talbot-VCSEL has not been enough considered so far, detailed conditions such as the influence of the amount of wavelength detuning and the number of required array size should be evaluated by numerical analysis.

3. Basic Analysis using Numerical Analysis Tool

3.1 Analysis Methods and Device Parameters

The analysis is based on differential equations called laser rate equations. In order to analyse the basic behaviour characteristics of mutual injection locking, we ignored carrier diffusion, time delay between lasers, and Langevin noise. In addition, a single mode operation, linear optical gain with respect to carrier density, and the uniform electric field and carrier density in the active region of each VCSEL are assumed. Table 1 shows typical parameters and their values of VCSEL used for this analysis.[27]

3.2 Numerical Analysis of Two Lasers

At first, in order to confirm the validity of analysis method and to clarify basic tendency of mutual injection locking, two lasers case (laser-1 and laser-2) was analyzed. The rate equation is as follows.

$$\frac{dS_i(t)}{dt} = \left[\Gamma G_{0i}(N_i(t) - N_{tr}) - \frac{1}{\tau_p}\right] S_i(t) + 2\kappa k_c \sqrt{S_i(t)S_j(t)} \cos\left(\Delta\phi_{ij}(t)\right) + \Gamma R_{sp} \quad (2)$$

$$\omega_i(t) = \frac{d\phi_i(t)}{dt} = \omega_{0i} + \frac{\alpha}{2}\left[\Gamma G_{0i}(N_i(t) - N_{tr}) - \frac{1}{\tau_p}\right] + \kappa k_c \sqrt{\frac{S_j(t)}{S_i(t)}} \sin\left(\Delta\phi_{ij}(t)\right) \quad (3)$$

$$\frac{dN_i(t)}{dt} = \frac{I_i}{eV} - \frac{N_i(t)}{\tau_n} - G_{0i}(N_i(t) - N_{tr})S_i(t) \quad (i,j = \{1,2\}\ i = \bar{j}) \quad (4)$$

Here κ is the injection ratio that means the ratio of how much the light emitted from one laser is injected into another laser and satisfies $0 \leq \kappa \leq 1$ and k_c is called coupling coefficient and represented by following equation.[16]

$$k_c = \frac{c}{2\eta_{eff}L} \frac{1-R}{R} = 1.45 \times 10^{11} \ [1/s]$$

Subscript 1 and 2 indicates parameters for laser-1 and laser-2, respectively. Temporal development of simultaneous rate equations for each laser was analysed by using the fourth order explicit Runge-Kutta method. Analysis was performed by using MATLAB program.

As the first analysis procedure, for each laser, the density of photon and carrier in the steady state before mutual injection that means independent operation were calculated and set as the initial state of analysis.

Then the temporal development of the density of photon and carrier and phase of each element was calculated until a sufficient time of 10 ns. After that, if wavelength difference $|\Delta\lambda| = |\lambda_1 - \lambda_2| = 2\pi c \left| \frac{1}{\omega_1} - \frac{1}{\omega_2} \right|$ is less than or equal to 0.01×10^{-12} m, these two lasers are determined to be locked. These procedures are implemented while varying the wavelength of laser-1 from 979.8 to 980.2 nm and injection ratio κ from 0.01 to 0.1. The wavelength of laser-2 is fixed at 980 nm. Figure 2 shows the locking range for both the initial wavelength detuning $\Delta\lambda_0 (= \lambda_{01} - \lambda_{02})$ of two lasers and the injection ratio κ. In this Figure, two lasers were set to the same operating conditions such as operation current, gain, initial photon and carrier density except for the difference in initial wavelength. In the injection locking of the master-slave scheme, it is well known that the locking range is asymmetric with respect to the wavelength detuning 0. However, due to the mutual injection locking under equal conditions between two lasers, the locking range is substantially symmetric with respect to the wavelength detuning 0.

Figure 3 shows the locking range when $I_1 = 23$ mA and $I_2 = 35$ mA. The locking range becomes shrink and mainly exists only in $\Delta\lambda_0 < 0$. This situation is similar to an injection locking of master-slave scheme.[19] This is because that for the laser-1 with lower current and lower intensity of light the injected light into the laser-1 is relatively larger compared to the injected light into the laser-2. Therefore, laser-1 is more affected and the wavelength of laser-1 shifted largely to longer side. As the result in the case of two lasers with asymmetric operation condition, a laser driven by lower current should have shorter initial wavelength and the other laser driven by higher current should have longer initial wavelength.

While locking range in Fig. 3 is narrow as compared to Fig. 2, even with lower injection

ratio such as $\kappa < 0.5$, it can be locked at a large wavelength detuning shown as red marker. This means locking range expands in a part. This result suggests that in the case of mutual injection locking, there is a possibility of locking even for larger wavelength detuning by adjusting the injection current.

3.3 Numerical Analysis of Three Lasers

Next, we analyzed mutual injection locking in three lasers to discuss more complicated dependency than in the case of two lasers. The rate equation is modified as follows.

$$\frac{dS_i(t)}{dt} = \left[G_{0i}(N_i(t) - N_{tr}) - \frac{1}{\tau_p} \right] S_i(t) + 2\kappa k_c \sqrt{S_i(t)S_j(t)} \cos(\Delta\phi_{ij}(t)) + $$
$$2k_{cik}\sqrt{S_i(t)S_k(t)} \cos(\Delta\phi_{ik}(t)) + R_{sp} \qquad (5)$$

$$\omega_i(t) = \frac{d\phi_i(t)}{dt} = \omega_{0i} + \frac{\alpha}{2}\left[G_0(N_i(t) - N_{tr}) - \frac{1}{\tau_p} \right] + k_{cij}\sqrt{\frac{S_j(t)}{S_i(t)}} \sin(\Delta\phi_{ij}(t)) + $$
$$\kappa k_c \sqrt{\frac{S_k(t)}{S_i(t)}} \sin(\Delta\phi_{ik}(t)) \qquad (6)$$

$$\frac{dN_i(t)}{dt} = \frac{I_i}{eV} - \frac{N_i(t)}{\tau_n} - G_{0i}(N_i(t) - N_{tr})S_i(t) \quad (i,j,k = \{1,2,3\}) \quad (7)$$

Figure 4 shows the locking range dependence on wavelength detuning of $\Delta\lambda_{12}$ (= λ_{01}-λ_{02}) and $\Delta\lambda_{32}$ (= λ_{03}-λ_{02}). The wavelength of laser-2 is fixed at 980 nm and the wavelengths of the lasers-1 and -3 are varied from 979.8 to 980.2 nm, respectively. Since the lasers-1 and -3 are symmetrical, the locking range is also symmetrical in condition of *y=x* of *x* and *y* axis. When the initial wavelengths of two lasers are equal as shown in blue solid lines, the locking range is expanded. In other words, if there are elements whose wavelengths are identical or close to each other, the locking range is expanded. Thus, it is expected that the locking range can be expanded by increasing the size of array.

4. Numerical Analysis of N×N VCSEL Array

4.1 Method

First, coordinate axes of x-y-z are set as follows. The center of the light source array is the origin, and the array plane corresponds to the x-y plane. The direction toward the reflector is the plus direction of z-axis. As a Talbot-VCSEL, we analyzed the mutual injection locking

of N×N lasers arranged in 2D array. We should note that since Talbot-VCSEL uses reflected light as injection light into each other, the rate equations include self-feedback light as shown in following equations.

$$\frac{dS_i(t)}{dt} = \left[\Gamma G_{0i}(N_i(t) - N_{tr}) - \frac{1}{\tau_p}\right] S_i(t) + \sum_{j=1}^{N^2} 2\kappa_{ij} k_c \sqrt{S_i(t) S_j(t)} \cos\left(\phi_j(t) - \phi_i(t) + \theta_{ij}\right) + \Gamma R_{sp} \quad (8)$$

$$\omega_i(t) = \frac{d\phi_i(t)}{dt} = \omega_{0i} + \frac{\alpha}{2}\left[\Gamma G_{0i}(N_i(t) - N_{tr}) - \frac{1}{\tau_p}\right] + \sum_{j=1}^{N^2} \kappa_{ij} k_c \sqrt{\frac{S_j(t)}{S_i(t)}} \sin\left(\phi_j(t) - \phi_i(t) + \theta_{ij}\right) \quad (9)$$

$$\frac{dN_i(t)}{dt} = \frac{I_i}{eV} - \frac{N_i(t)}{\tau_n} - G_{0i}(N_i(t) - N_{tr})S_i(t) \quad i = 1, 2, \dots N^2 \quad (10)$$

where κ_{ij} is the coupling ratio of the light injected from laser-*j* to laser-*i*. This κ_{ij} is calculated by integrating the irradiated light intensity distribution over the aperture area of the element (laser-*i*). The light is after propagation of distance *z* of one laser (laser-*j*) which has a Gaussian beam and the intensity is normalized. The equation is as shown the following.

$$\kappa_{ij} = \iint_{S_{xy}} |E_z(x, y)| dx dy \quad (11)$$

where $E_z(x, y)$ is the Gaussian beam after propagation of distance *z* derived by Fresnel Kirchhoff integral as follows.

$$E_z(x, y) = \frac{w_0}{W_z} \exp\left\{-\frac{(x-x_0)^2 + (y-y_0)^2}{W_z^2}\right\} \exp\left\{-jk\left(z + \frac{(x-x_0)^2 + (y-y_0)^2}{2R_z} - \frac{\Phi}{k}\right)\right\} \quad (12)$$

Here, $W_z = w_0 \sqrt{1 + \left(\frac{2z}{kw_0^2}\right)^2}$, $R_z = z\left[1 + \left(\frac{kw_0^2}{2z}\right)^2\right]$, $\Phi = \tan^{-1}\frac{2z}{kw_0^2}$. W_z represents the beam spot size of the Gaussian beam at the distance *z*, and R_z represents the radius of curvature of the equiphase surface of the Gaussian beam at the distance *z*, (x_0, y_0) is the coordinate of emission laser-j and (x, y) is the coordinate of irradiated laser-i. θ_{ij} is the phase rotation by propagation of the light injected from laser-j to laser-i and calculated by the phase part of above Gaussian beam as shown below.

$$\theta_{ij} = k\left(z + \frac{(x-x_0)^2 + (y-y_0)^2}{2R_z} - \frac{\Phi}{k}\right) \quad (13)$$

The initial wavelengths are set randomly with a normal distribution with standard deviation $\sigma = \Delta\lambda_{0max}/2 = 0.1/2$ nm and the initial phases are set randomly with a uniform distribution from $-\pi$ to π.

4.2 Result

We analyzed the injection locking characteristics depending on array pitch, VCSEL aperture diameter, array size, and propagation distance of twice of the reflector distance, which can be designed in actual device.

At first, analysis examples of the temporal development of the wavelength are shown as shown in Fig. 5. Figure is analyzed for 121 (11×11) lasers with an array pitch p of 30 μm and an aperture diameter D of 3 μm in the case of propagation distance z of z_t (Talbot distance). Although the wavelengths of the individual lasers slightly fluctuate due to mutual interference, wavelength locking, or reduction of wavelength detuning are not observed in the set condition.

Figure 6 shows the result of integration of the light intensity distribution (irradiated image) irradiated on the surface of the VCSEL array from 4.99 to 5 nanosecond. Center of the array is extracted. The irradiated intensity distribution $\psi_z(x, y)$ is greatly different from the Talbot image created by a finite number of elements that has coherent light. Here the correlation value (CV) is defined as the following formula in which $\psi_0(x, y)$ and $\psi_z(x, y)$ are intensity distribution before and after propagation. The CV for the calculated condition is very small as 0.94×10^{-3}.

$$CV = \frac{\iint \psi_0(x,y) * \psi_z(x,y) dxdy}{\iint \psi_0(x,y) * \psi_0(x,y) dxdy} \qquad (14)$$

Next, the temporal development of the wavelength in the case of an increased aperture diameter of 7 μm is shown in Fig. 7. The array size of 11×11 with an array pitch of 30 μm is the same as previous.

Unlike the small aperture results, some of the wavelengths greatly interfere with each other immediately after mutual injection and then some wavelengths periodically vary on the longer wavelength side (around 980.2 nm). The other several wavelengths that do not

coincide with the group in longer side fluctuate greatly near the initial wavelength of about 980 nm in Fig. 7.

The wavelengths that were random before mutual injection are locked after injection at around 980.2 nm as shown in Fig. 7 (b). The locked wavelengths consist of two modes that periodically fluctuate their wavelengths alternatively. Figure 8 shows an array distribution of wavelength and phase before and after mutual injection under this condition. The locking is also confirmed from the checked pattern of the wavelength as shown in the Fig. 8(d). This is equivalent to the fact that the threshold gains of the in-phase mode and the out-phase mode are considered to be approximately equal and minimum in the configuration with the cavity length of zt which is half of Talbot distance.[28] The irradiated intensity distribution in this case is close to the ideal Talbot image as shown in Fig. 9. In addition, the CV is large as 0.212.

In the case of the propagation distance z_t, there are mainly two modes of the wavelength distribution in a steady state. On the other hand, at the fraction of Talbot distance such as $z_t/2$ or $z_t/4$, is is known that the original image is also re-imaged[24, 25] so the locking characteristics for propagation distances $z_t/2$ and $z_t/4$ were also evaluated. Figures 10-12 show the result for propagation distance $z = z_t/2$ (reflector position $z_t/4$). The other parameters are 11×11 array, array pitch of 50 μm, and aperture diameter of 5 μm.

Unlike the case of the propagation distance of z_t, the wavelength distribution mainly converges to one mode with longer wavelength and the out-phase mode dominates in phase distribution. Note that the elements whose wavelengths do not coincide largely fluctuate on the shorter wavelength side and the phases do not coincide.

Figure 13-15 show the result for propagation distance $z = z_t/4$ (reflector position $z_t/8$). The other parameters are 11×11 array, array pitch of 80 μm, aperture diameter of 7 μm.

The wavelengths and phases after injection locking are mainly consistent with one value except for the elements with large initial wavelength detuning (represented by deep yellow or blue in Fig. 14 upper-right). This is considered to be equivalent to the fact that the threshold gain of in-phase mode is smallest when the propagation distance is $z_t/4$.[27] The amount of transition to the longer wavelength side of the locked wavelength group is smaller than other analysis conditions such as at z_t and $z_t/2$. This is because the intensity of the ideal Talbot image at $z_t/4$ is small and it may causes that the intensity of incomplete Talbot image

at $z_t/4$ is also small.[28, 29)]

4.3 Discussion

The above analysis was performed and evaluated for various array pitches, aperture diameters, number of elements (array size), and propagation distance (2×reflector distance). Figures 16, 18, 19 show analysis results of *CV* for various aperture diameters of 3, 5, and 7 μm.

From these results, it is found that the *CV* becomes to be higher as the aperture diameter is larger. At propagation distance zt, in case the aperture diameter is small (< 3 μm), locking operation was not observed with any array pitch (very low *CV*). As the array pitch is smaller and the aperture diameter is larger, then the *CV* becomes larger at the propagation distance z_t. In order to obtain a large *CV* of > 0.1, the conditions of aperture diameter of > 5 μm and array pitch of < 30 μm are necessary. The tolerance of the position of Talbot-mirror is shown in Fig. 17. This figure shows the relationship between *CV* and propagation distance in case that the array number, the aperture diameter and the array pitch are 11×11, 5 μm and 30 μm. *CV* is seen to be increased within a range of about 0.8 mm at around the Talbot-distance of about 1.8 mm. This means a Talbot-mirror can be arranged with some realistic tolerance.

On the other hand, in the case propagation distance is $z_t/2$ or $z_t/4$, a large *CV* can be obtained even with a relatively wide array pitch of > 70 μm. This is because that the Talbot distance increases with the wider array pitch as expressed by Talbot distance in Equation (1), however by setting the propagation distance to a fraction of the Talbot distance, it is possible to satisfy that the propagation distance is less than the effective coherence length corresponding to the wavelength detuning of the array.[30)] Regardless of the array pitch, there is a certain propagation distance for locking. However, with small aperture diameter of < 3 μm, *CV* decreases greatly with large array pitch as shown in Fig. 18 and 19. A certain degree of the aperture diameter is necessary for locking. This may be because amount of injection light is reduced due to small aperture.

Finally, we evaluated the relationship between the *CV* and the array size as shown in Fig. 20. As the tendency, the *CV* can be increased by increasing the number of arrays. However, in the case that array pitch is 30 μm, *CV* is saturated at the array size of 9×9. The intensity of ideal Talbot image of coherent light source is also saturated for array size, ease of locking

also will be saturated for large array size.

5. Conclusions

The operating conditions and structural design that are necessary to realize Talbot-VCSEL were studied by numerical analysis of mutual injection locking by using the laser rate equation. Analysis of a few elements confirms the tendency of mutual injection locking and shows that the locking range can be expanded by increasing the number of elements which have close wavelength. Furthermore, Talbot-VCSEL of a two-dimensional array was analyzed to clarify the optimal array configuration that are necessary for locking operation. As the results, the aperture diameter of > 5 μm and the array size of > 9×9 with 30 μm of array pitch is appropriate minimum configuration of the 2D VCSEL array.

The above analysis results indicate that Talbot-VCSEL can be realized by a feasible configuration in actual device fabrication. We proceed with investigation of experimental verification. The observed results and future experimental confirmation will help realization of a high power and high quality beam light source for various applications.

Acknowledgments

References

1) M. Hirota, S. Iio, Y. Ohta, and T. Miyamoto, Tech. Dig. 20th Microoptics Conf., 2015, H86.
2) T. Miyamoto, Proc. SPIE **10682**, 1068204 (2018).
3) Y. Katsuta and T. Miyamoto, Jpn. J. Appl. Phys. **57**, 08PD01 (2018).
4) A. C. Lehman and K. D. Choquette, IEEE Photon. Technol. Lett. 19, 1421 (2007).
5) L. D. A. Lundeberg, G. P. Lousberg, D. L. Boiko, and E. Kapon, Appl. Phys. Lett. **90**, 021103 (2007).
6) M. Xun, C. Xu, Y. Xie, Y. Zhu, M. Mao, K. Xu, J. Wang, J. Liu, and H. Chen, Electron. Lett. **50**, 1085 (2014).
7) S. T. M. Fryslie, M. T. Johnson, and K. D. Choquette, IEEE J. Quant. Electron. **51**, 2600206 (2015).
8) Z. Gao, B. J. Thompson, G. Ragunathan, M. T. Johnson, B. Rout, and K. D. Choquette, IEEE Photon. Technol. Lett. **28**, 513 (2016).
9) G. Pan, Y. Xie, C. Xu, M. Xun, Y. Dong, J. Deng, and H. Chen, IEEE J. Quant. Electron. **54**, 2400306 (2018).
10) M. Imada, S. Noda, A. Chutinan, T. Tokuda, M. Murata, and G. Sasaki, Appl. Phys. Lett. **75**, 316 (1999).
11) H. J. Unold, M. Golling, R. Michalzik, D. Supper, and K. J. Ebeling, Proc. 27th European Conf. Optical Comm., 2001, Th.A.1.4.
12) N. Yokouchi, A. J. Danner, and K. D. Choquette, IEEE J. Select. Tops. Quant. Electron. **9**, 1439 (2003).
13) K. Hirose, Y. Liang, Y. Kurosaka, A. Watanabe, T. Sugiyama, and S. Noda, Nature Photon. **8**, 406 (2014).
14) E. Ho, F. Koyama, and K. Iga, Appl. Optics **29**, 5080 (1990).
15) T. Shichijo and T. Miyamoto, Tech. Dig. 23rd Microoptics Conf., 2018, P-62.
16) N. Schunk and K. Petermann, IEEE J. Quant. Electron. **22**, 642 (1986).
17) M. S. Torre, C. Masoller, and K. A. Shore, IEEE J. Quant. Electron. **40**, 25 (2004).
18) H. Li, T. L. Lucas, J. G. McInerney, M. W. Wright, R. A. Morgan, IEEE J. Quant. Electron. **32**, 227 (1996).
19) J. Y. Law, G. H. M. van Tartwijk, and G. P. Agrawal, J. European Opt. Soc. Part B **9**, 737 (1997).
20) Z. Chen, J. Hou, P. Zhou, X. Wang, X. Xu, Z. Jiang, and Z. Liu, Opt. Comm. **282**, 60 (2009).
21) J. Mulet, C. Mirasso, T. Heil, and I. Fischer, J. Opt. B **6**, 97 (2003).
22) R. M. Kurtz, R. D. Pradhan, T. M. Aye, G. D. Savant, T. P. Jannson, and L. G. DeShazer, IEEE J. Sel. Tops. Quant. Electron. **11**, 578 (2005).
23) H. F. Talbot, The London, Edinburgh, and Dublin Philosophical Mag. and J. Sci. **9**, 401 (1836).
24) L. Rayleigh, The London, Edinburgh, and Dublin Philosophical Mag. and J. Sci. **11**, 196 (1881).
25) J. Wen, Y. Zhang, and M. Xiao, Advances in Opt. and Photon. **5**, 83 (2013).
26) W. B. Case, M. Tomandl, S. Deachapunya, and M. Arndt, Opt. Exp. **17**, 20966 (2009).
27) L. A. Coldren, S. W. Corzine, M. L. Mashanovitch, *Diode Lasers and Photonic Integrated Circuits* (John Wiley & Sons, 2012) 2nd ed.
28) D. Mehuys, W. Streifer, R. G. Waarts, and D. F. Welch, Opt. Lett. **16**, 823 (1991).

29) Y. Komori and T. Miyamoto, Ext. Abstr. (The 64th JSAP Spring Meet.), 2017, 15a-422-12 [in Japanese].

30) Y. Komori and T. Miyamoto, Ext. Abstr. (The 63rd JSAP Spring Meet.), 2016, 20a-S321-5 [in Japanese].
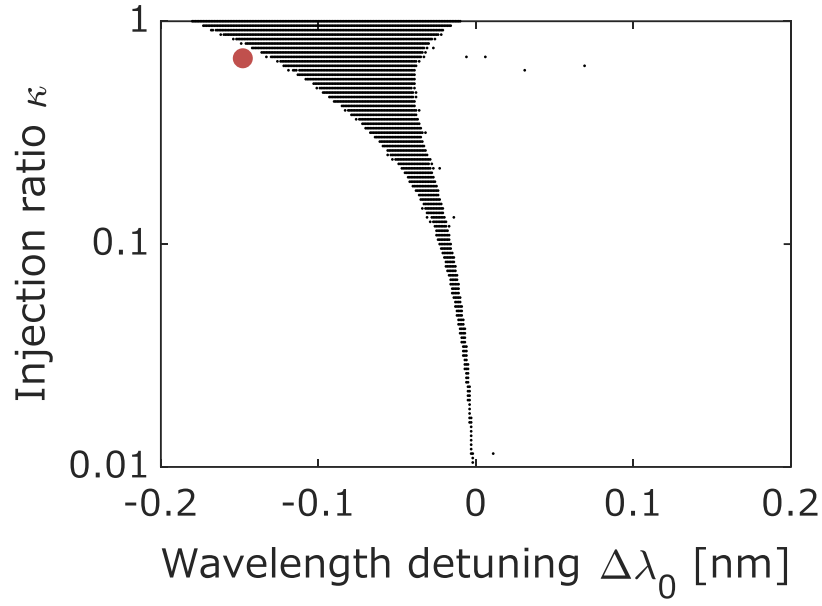
Figure Captions
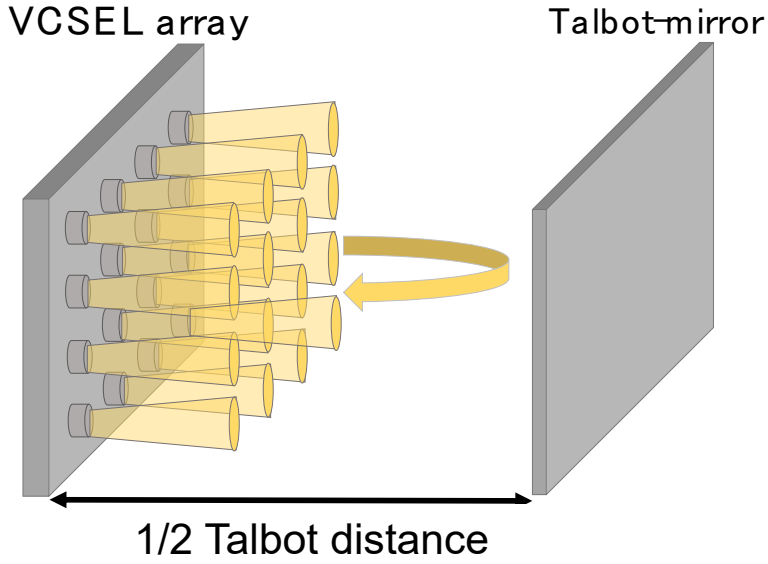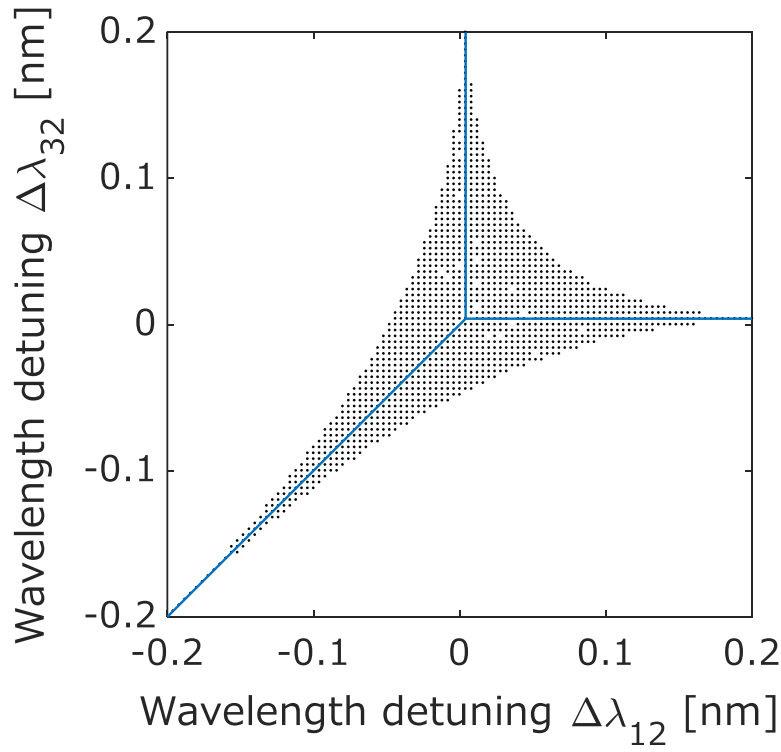

Fig. 1. Conceptual configuration of Talbot-VCSEL
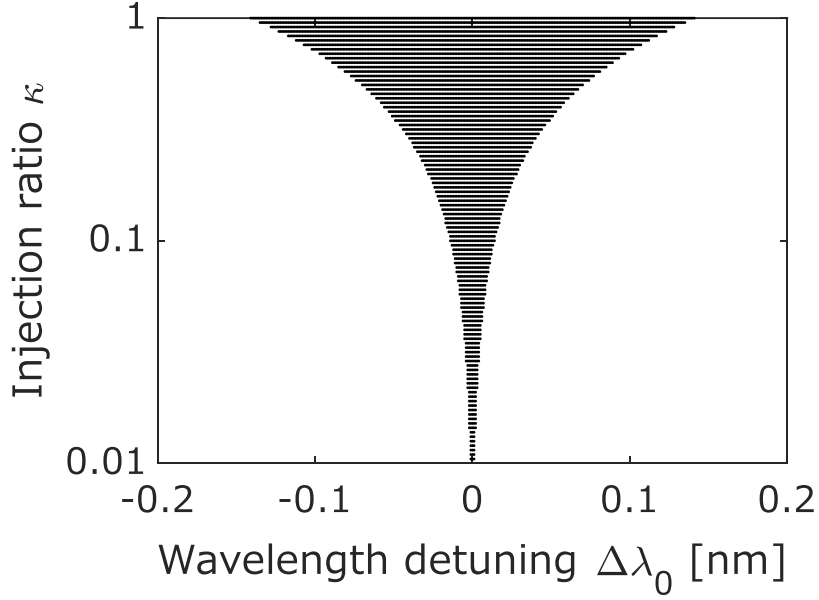
Fig. 2. Locking range dependence on the initial wavelength detuning $\Delta\lambda_0$ and the injection ratio κ of two lasers under I_1=23 mA and I_2=23 mA.

Fig. 3. Locking range dependence on the initial wavelength detuning $\Delta\lambda_0$ and the injection ratio κ of two lasers under I_1=23 mA and I_2= 35 mA.

Fig. 4. Locking range of three lasers for wavelength detuning of $\Delta\lambda_{12}$ and $\Delta\lambda_{32}$.
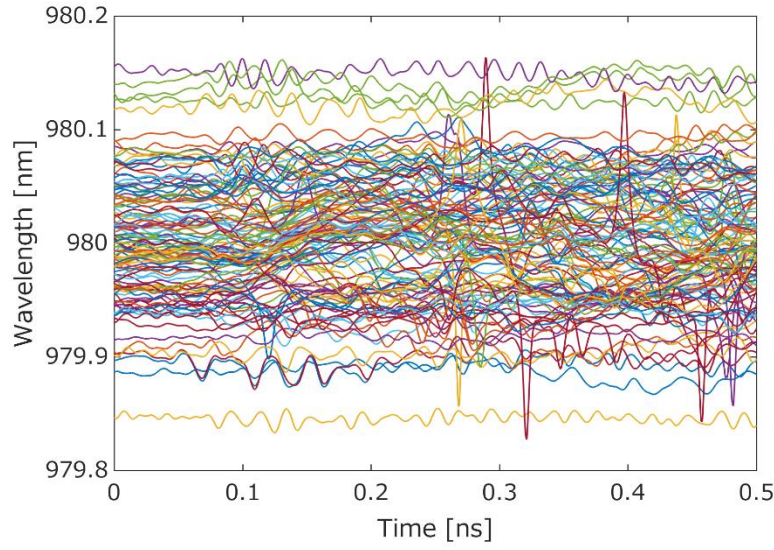
Fig. 5. Temporal development of the wavelength for 11×11 lasers with p=30 μm and D=3 μm, z=z_t.
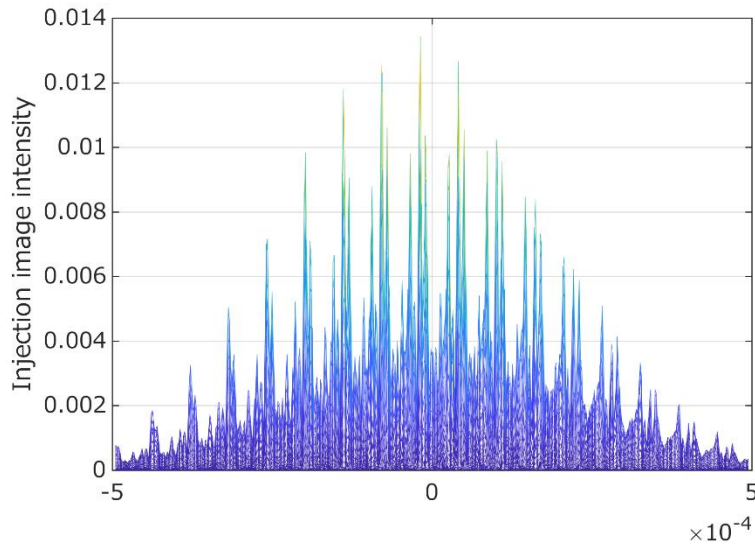
Fig. 6. Integrated irradiated intensity distribution for 11×11 lasers with p=30 μm and D=3 μm, z=z_t.
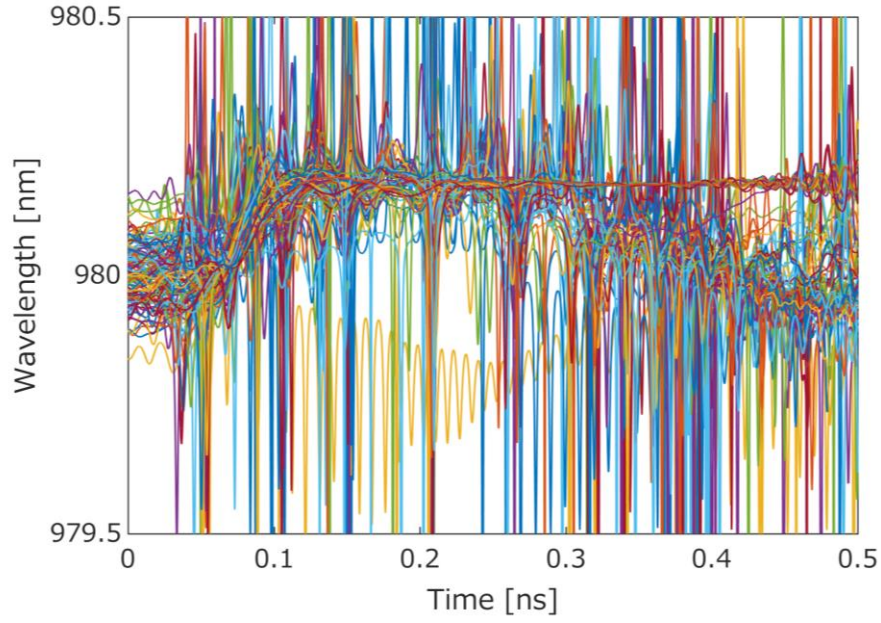
(a)
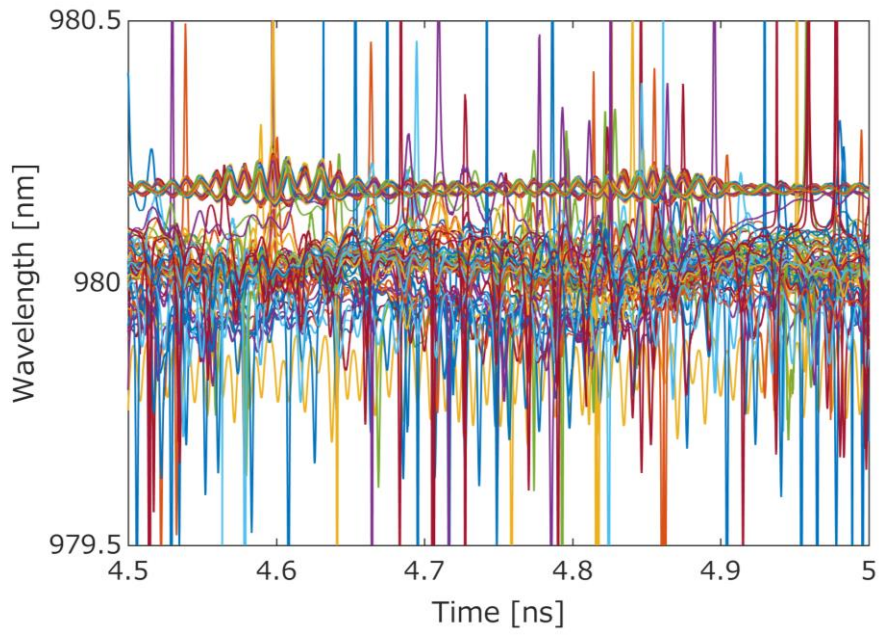
(b)

Fig. 7. Temporal development of the wavelength for 11×11 lasers with p=30 μm and D=7 μm, z=z_t. (a) from 0 to 0.5 ns, (b) from 4.5 to 5.0 ns.

(a) Phase before injection (b) Wavelength before injection

(c) Phase after injection (d) Wavelength after injection
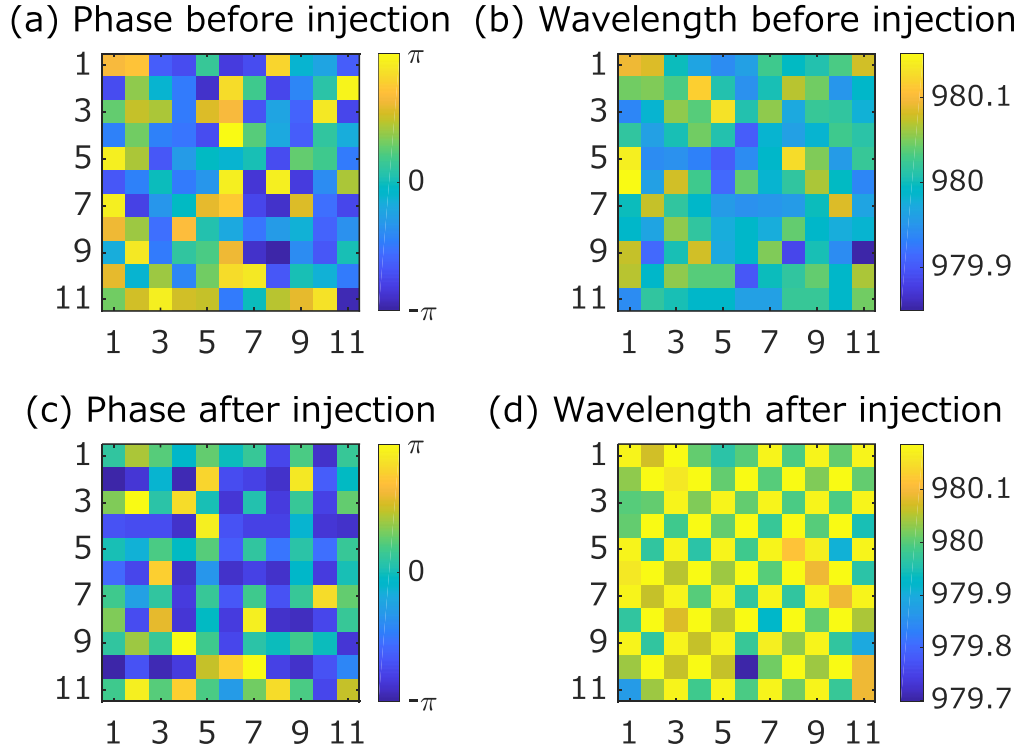
Fig. 8. Phase and wavelength distribution in array for 11×11 lasers with p=30 μm, D=7 μm, and z=z_t. (a) distribution of phase before mutual injection (b) wavelength before injection (c) phase after injection (d) wavelength after injection.
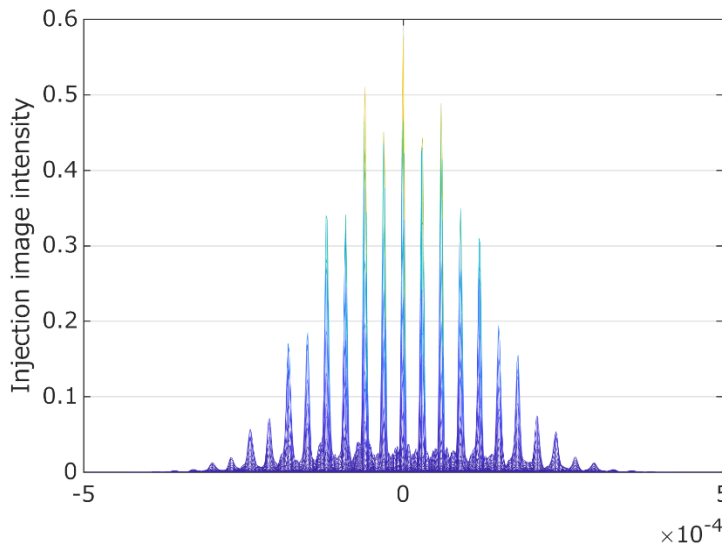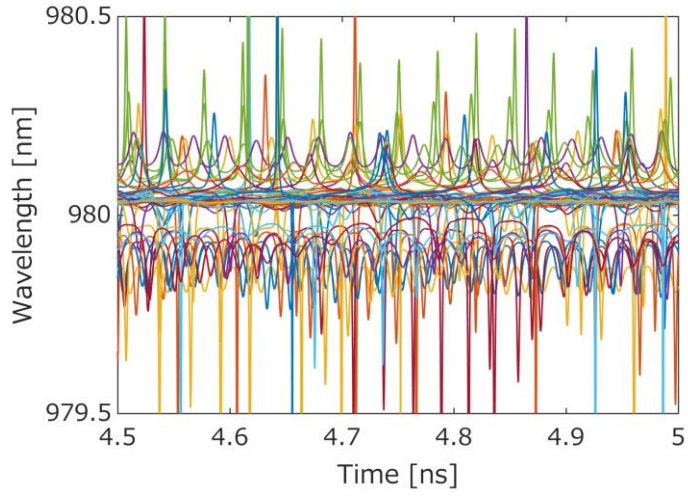

Fig. 9. Integrated irradiation intensity distribution for 11×11 lasers with p=30 μm and D=7 μm, z=z_t.
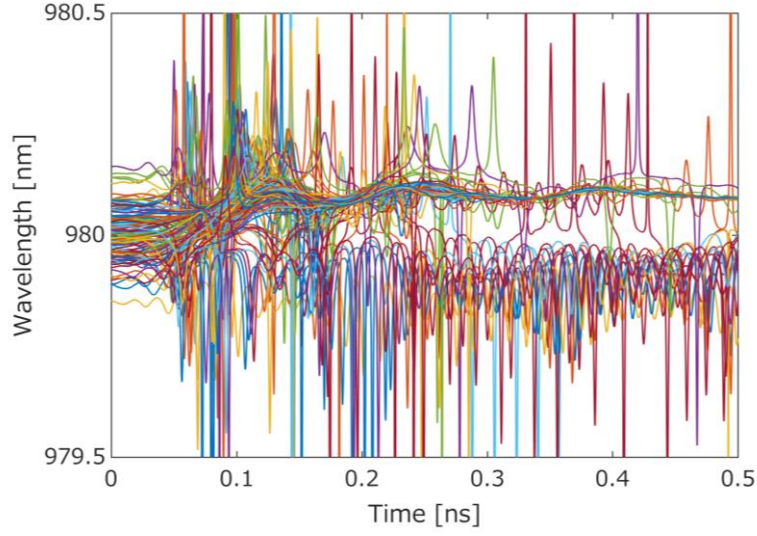
(a)
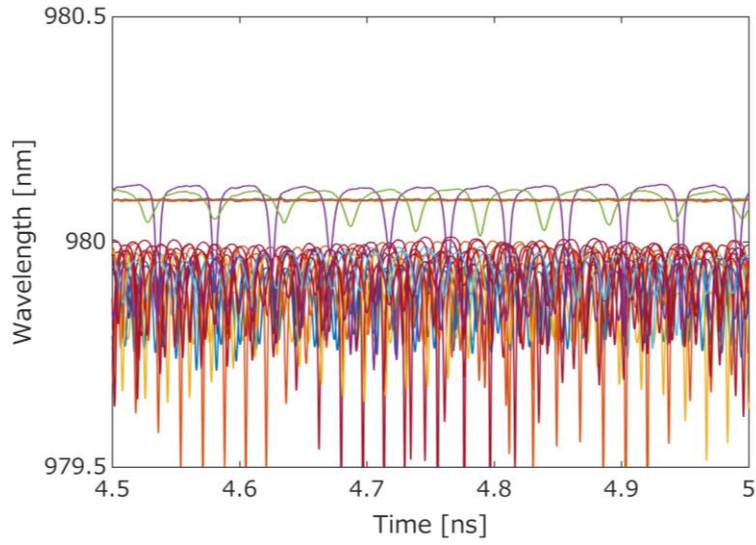
(b)

Fig. 10. Temporal development of the wavelength for 11×11 lasers with p=50 μm and D=5 μm, z=z_t/2. (a) from 0 to 0.5 ns, (b) from 4.5 to 5.0 ns.

Phase before injection   Wavelength before injection

Phase after injection   Wavelength after injection
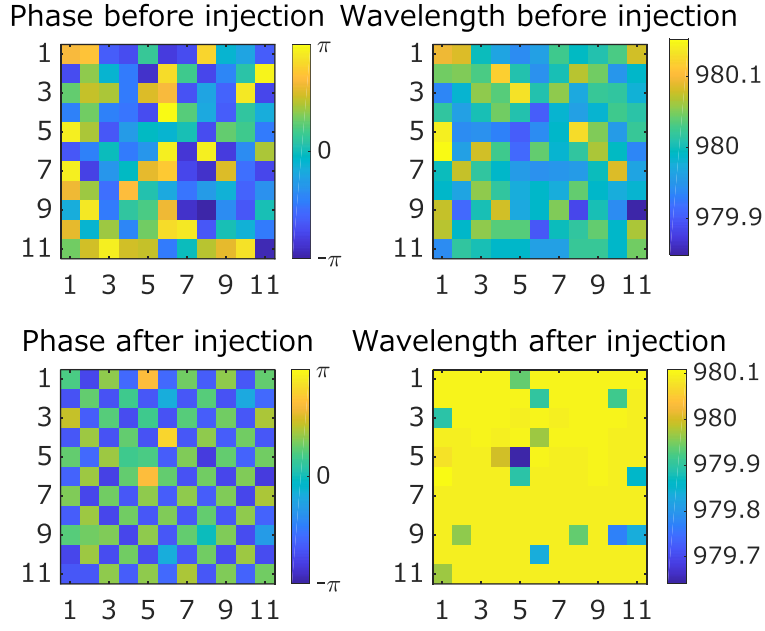
(a) (b)

(c) (d)

Fig. 11. Phase and wavelength distribution in array before and after mutual injection for 11×11 lasers with p=50 μm and D=5 μm, z=z_t/2. (a) distribution of phase before mutual injection (b) wavelength before injection (c) phase after injection (d) wavelength after injection.
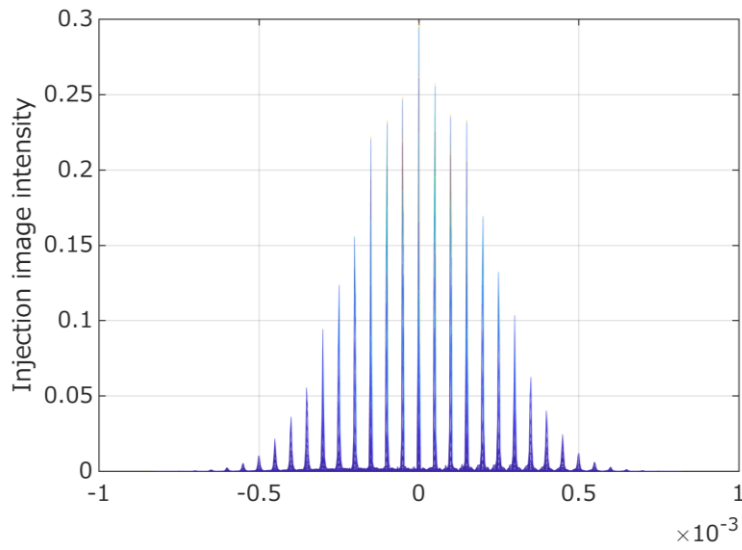

Fig. 12. Integrated irradiation intensity distribution for 11×11 lasers with p=50 μm and D=5 μm, z=z_t/2.
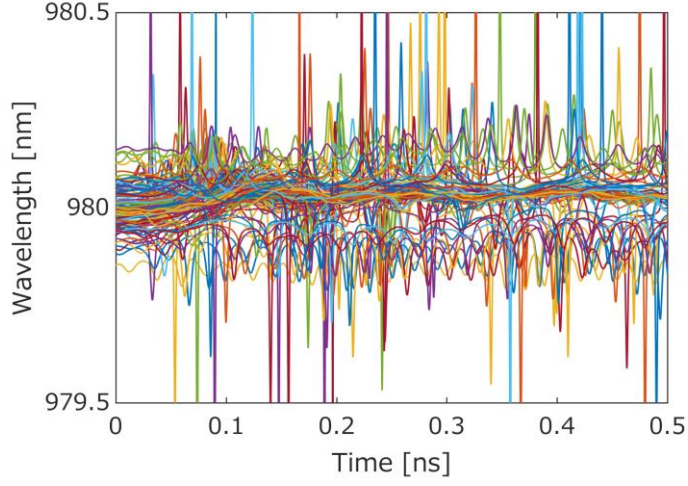
Fig. 13. Temporal development of the wavelength for 11×11 lasers with p=80 μm and D=7 μm, z=z_t/4. (a) from 0 to 0.5 ns, (b) from 4.5 to 5.0 ns.
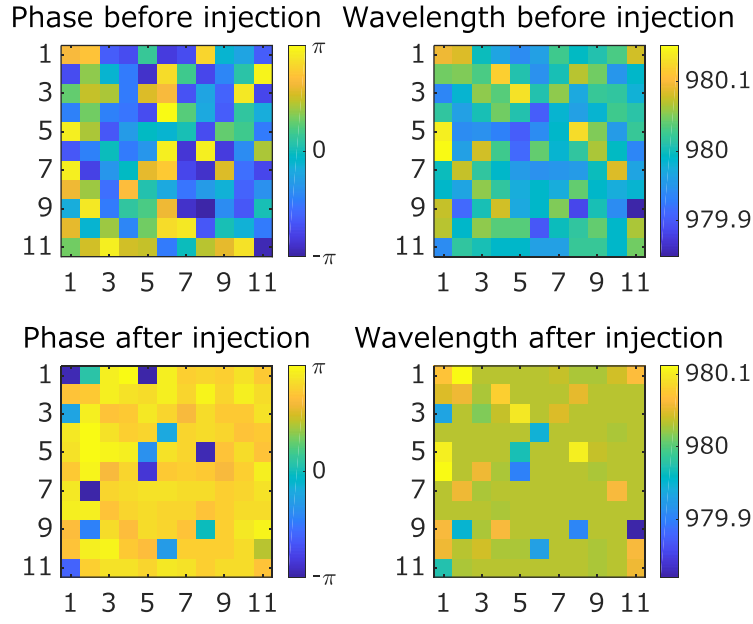
Fig. 14. Phase and wavelength distribution in array before and after mutual injection for 11×11 lasers with $p=80$ μm and $D=7$ μm, $z=z_t/4$. (a) distribution of phase before mutual injection (b) wavelength before injection (c) phase after injection (d) wavelength after injection.
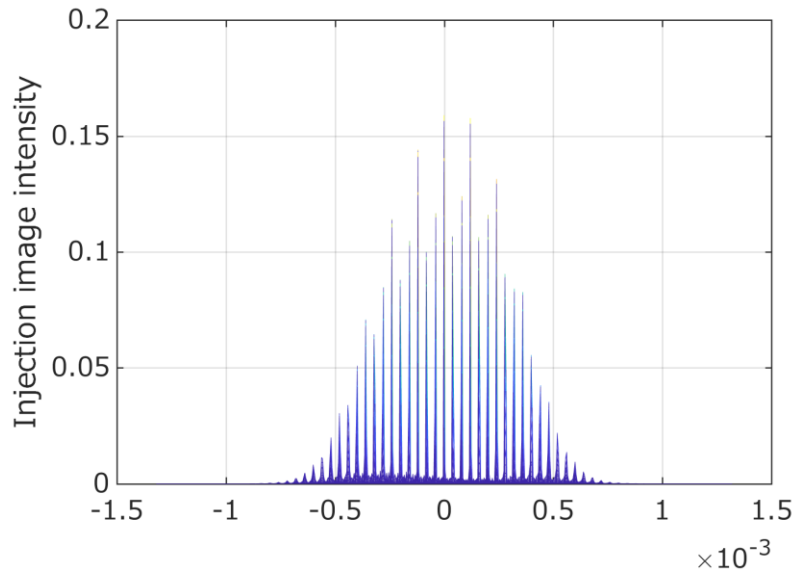
Fig. 15. Integrated irradiation intensity distribution for 11×11 lasers with p=80 μm and D=7 μm, z=z_t/4.
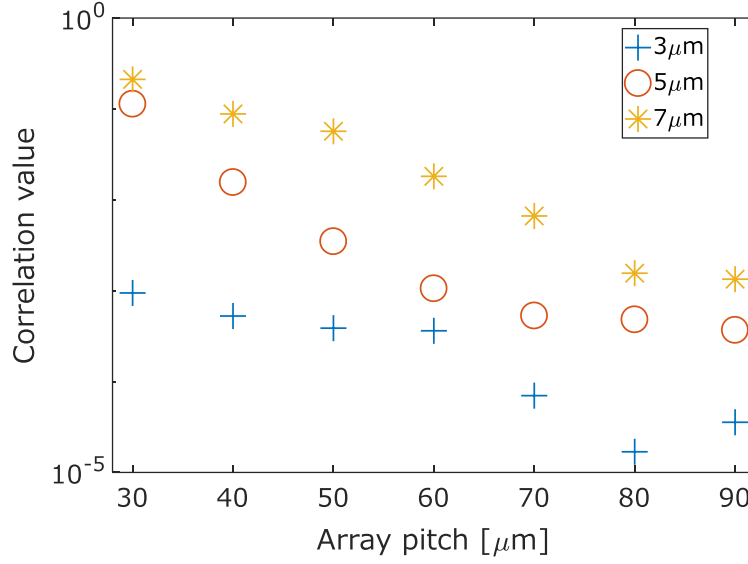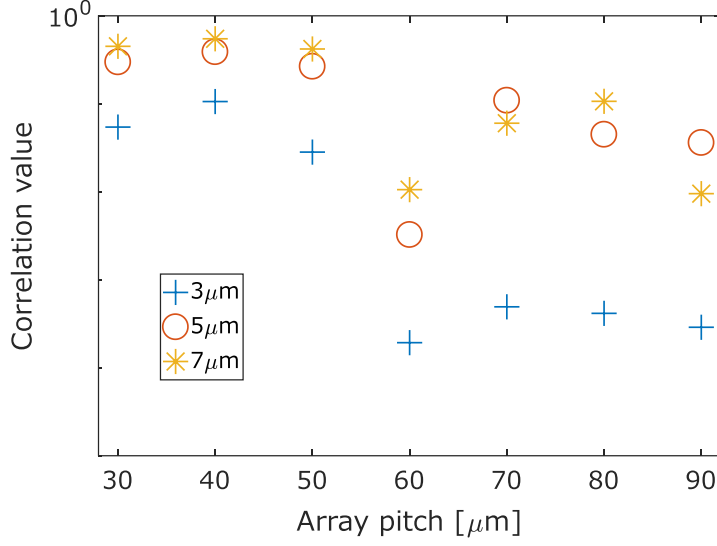

Fig. 16. *CV* vs. array pitch of 11×11 lasers for each D (3, 5, 7 μm) at z=z_t.
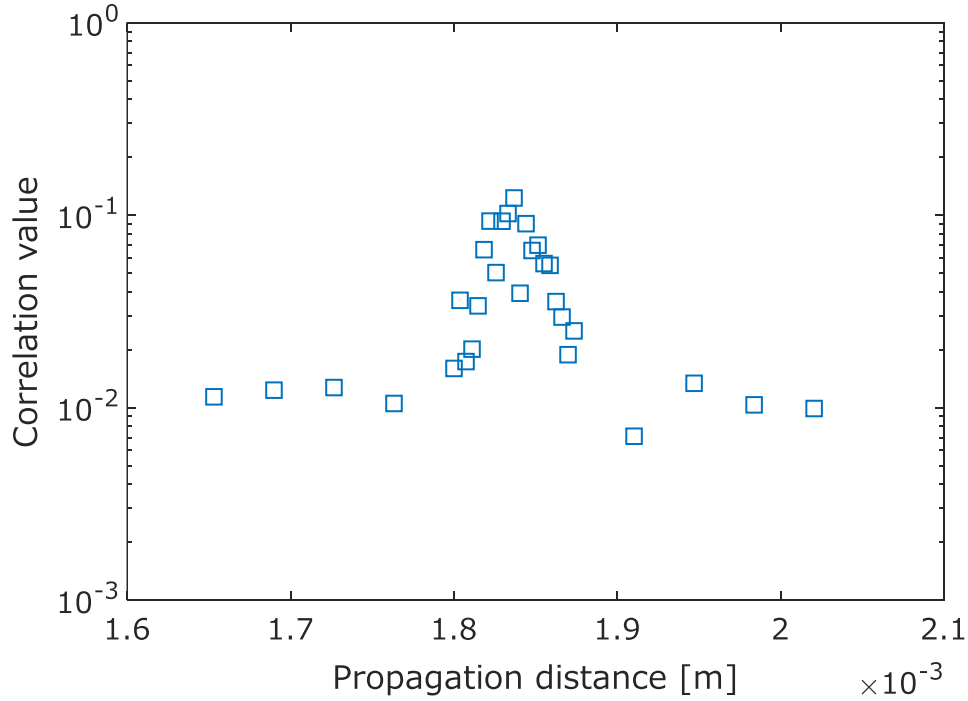
Fig. 17. *CV* vs. propagation distance for 11×11 lasers with p=30 μm and D=5 μm at around

$z=z_t.$

Fig. 18. *CV* vs. array pitch of 11×11 lasers for each *D* (3, 5, 7 μm) at *z=z_t*/2.
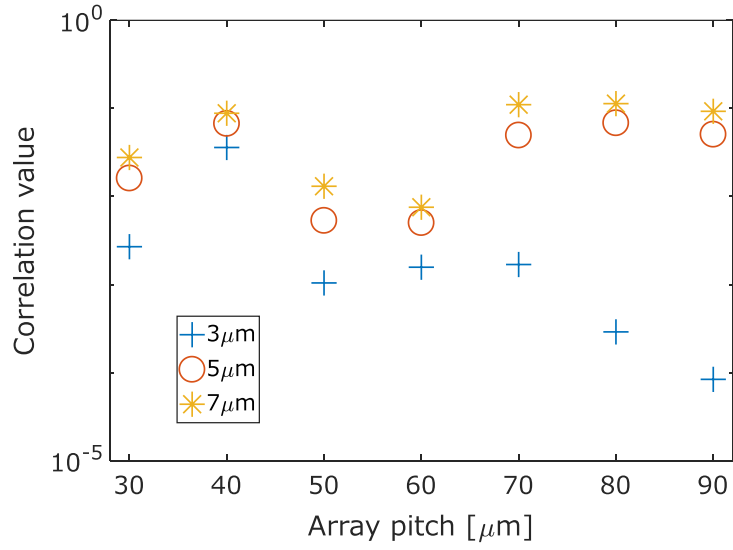
Fig. 19. *CV* vs. array pitch of 11×11 lasers for each *D* (3, 5, 7 μm) at *z=z_t*/4.

25
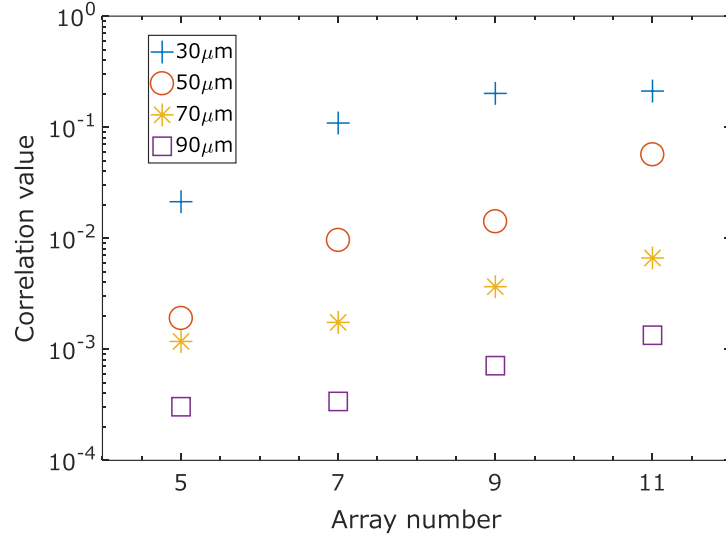
Fig. 20. *CV* vs. array size. Array number shows N of $N \times N$ array. with $D=7$ µm for each p (30, 50, 70, 90 µm) at $z=z_t$.

Table I. Parameters of a typical VCSEL used in analysis.

Parameter	Value
Linewidth enhancement factor	$\alpha = 5$
Differential gain coefficient	$G_{0i} = 1.76 \times 10^{-6}\ [\text{cm}^3/\text{s}]$
Transparent carrier density	$N_{tr} = 1.8 \times 10^{18}\ [\text{cm}^{-3}]$
Photon lifetime	$\tau_p = 2.2 \times 10^{-12}\ [\text{s}]$
Carrier lifetime	$\tau_n = 2.63 \times 10^{-9}\ [\text{s}]$
Driving current	$I = 2.32\ [\text{mA}]$
Spontaneous emission rate	$R_{sp} = 2.09 \times 10^{23}\ [\text{cm}^{-3}/\text{s}]$
Volume	$V = 2.4 \times 10^{-12}\ [\text{cm}^3]$
Confinement factor	$\Gamma = 0.038$
Coupling coefficient [16]	$k_c = 1.45 \times 10^{11}\ [1/\text{s}]$